

000
001
002054
055
056003

External Prior Guided Internal Prior Learning for Real Noisy Image Denoising

057
058004
005
006
007
008
009
010
011059
060
061
062
063
064
065

012 Anonymous CVPR submission

066

013 Paper ID 1047

067

Abstract

Most of existing image denoising methods use some statistical models such as additive white Gaussian noise (AWGN) to model the noise, and learn image priors from either external data or the noisy image itself to remove noise. However, the noise in real-world noisy images is much more complex than AWGN, and it is hard to be modeled by simple analytical distributions. Therefore, many state-of-the-art denoising methods in literature become much less effective when applied to real noisy images. In this paper, we develop a robust denoiser for real noisy image denoising without explicit assumption on noise models. Specifically, we first learn external priors from a set of clean natural images, and then use the learned external priors to guide the learning of internal latent priors from the given noisy image. The proposed method is simple yet highly effective. Experiments on real noisy images demonstrate that it achieves much better denoising performance than state-of-the-art denoising methods, including those designed for real noisy images.

1. Introduction

Image denoising is a crucial and indispensable step to improve image quality in digital imaging systems. In particular, with the decrease of size of CMOS/CCD sensors, noise is more easily to be corrupted and hence denoising is becoming increasingly important for high resolution imaging. In literature of image denoising, the observed noisy image is usually modeled as $\mathbf{y} = \mathbf{x} + \mathbf{n}$, where \mathbf{x} is the latent clean image and \mathbf{n} is the corrupted noise. Numerous image denoising methods [1, 2, 6, 3, 4, 5, 7, 8, 9, 10, 11, 12, 13] have been proposed in the past decades, including sparse representation and dictionary learning based methods [1, 2, 6], nonlocal self-similarity based methods [3, 4, 5, 6, 7], low-rank based methods [8], neural network based methods [9], and discriminative learning based methods [10, 11].

Most of the existing denoising methods [1, 2, 3, 4, 5, 6, 7, 8, 9, 10, 11, 12, 13] mentioned above assume noise \mathbf{n} to be additive white Gaussian noise (AWGN). Unfortunately, this assumption is too ideal to be true for real-world noisy im-

ages, where the noise is much more complex than AWGN [14, 15] and varies by different cameras and camera settings (ISO, shutter speed, and aperture, etc.). According to [15], the noise corrupted in the imaging process [is signal dependent and comes from five main sources: photon shot, fixed pattern, dark current, readout, and quantization noise. As a result, many advanced denoising methods in literature becomes much less effective when applied to real-world noisy images. Fig. 1 shows an example, where we apply some representative and state-of-the-art denoising methods, including CBM3D [5], WNNM [8], MLP [9], CSF [10], and TRD [11], to a real noisy image (captured by a Nikon D800 camera with ISO is 3200) provided in [14]. One can see that these methods either remain the noise or over-smooth the image details on this real noisy image.

There have been a few methods [16, 17, 18, 14, 19, 20, 21] developed for real noisy image denoising. Almost all of these methods follow a two-stage framework: first estimate the parameters of the assumed noise model (usually Gaussian or mixture of Gaussians (MoG)), and then perform denoising with the estimated noise model. Again, the noise in real noisy images is very complex and hard to be modeled by explicit distributions such as Gaussian and MoG. Fig. 1 also shows the denoised results of two state-of-the-art real noisy image denoising methods, Noise Clinic [19, 20] and Neat Image [21]. One can see that these two methods do not perform well on this noisy image either.

This work aims to develop a robust solution for real noisy image denoising without explicitly assuming certain noise models. To achieve this goal, we propose to first learn image priors from external clean images, and then employ the learned external priors to guide the learning of internal latent priors from the given noisy image. The flowchart of the proposed method is illustrated in Fig. 3. We first extract millions of patch groups from a set of high quality natural images, with which a Gaussian Mixture Model (GMM) is learned as the external prior. The learned GMM prior model is used to cluster the patch groups extracted from the given noisy image, and then a hybrid orthogonal dictionary (HOD) is learned as the internal prior for image denoising. Our proposed denoising method is simple and ef-

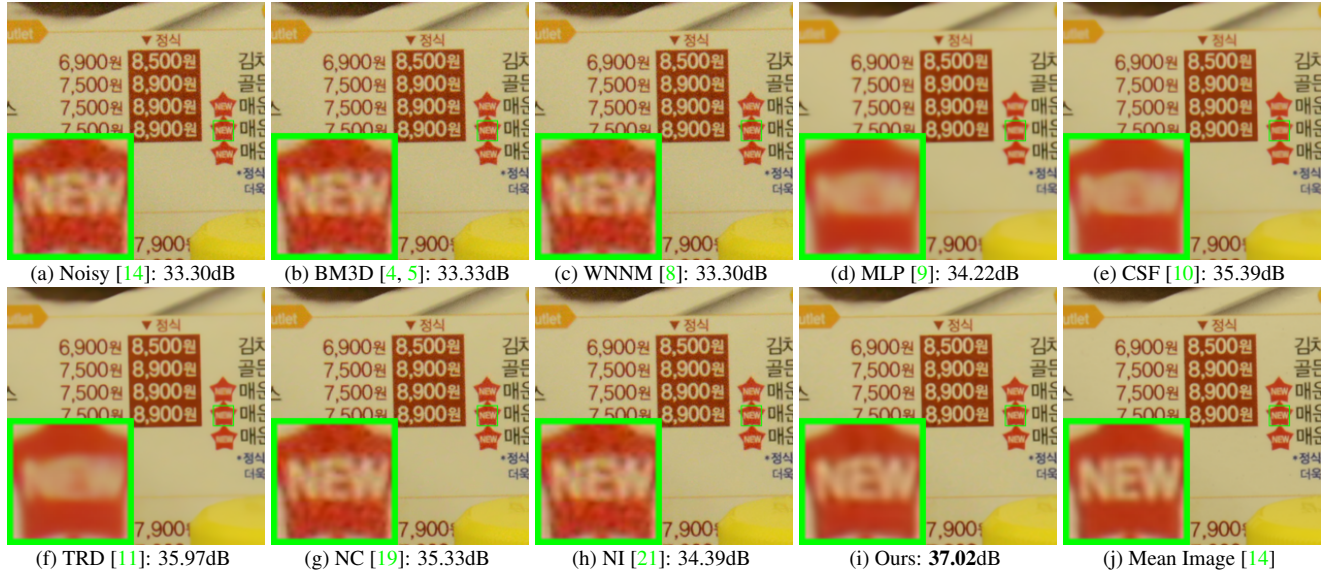


Figure 1. Denoised images of the real noisy image “Nikon D800 ISO 3200 A3” from [14] by different methods. The images are better viewed by zooming in on screen.

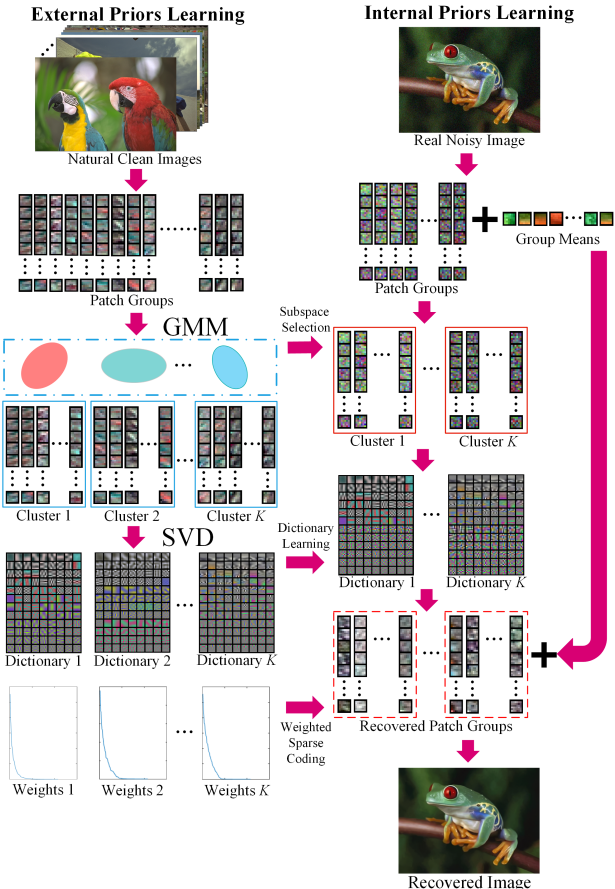


Figure 2. Flowchart of the proposed external prior guided internal prior learning and real noisy image denoising framework.

ficient, yet our extensive experiments on real noisy images clearly demonstrate its better denoising performance than the current state-of-the-arts.

2. Related Work

2.1. Internal vs. External Prior Learning

Image priors are playing a key role in image denoising [7, 13, 1, 23, 6, 22]. There are mainly two categories of prior learning methods. 1) External prior learning methods [12, 7, 13] learn priors (e.g., dictionaries) from a set of external clean images, and the learned priors are used to recover the latent clean image from noisy images. 2) Internal prior learning methods [1, 6, 23, 22] directly learn priors from the given noisy image, and the image denoising is often done simultaneously with the prior learning process. It has been demonstrated [7, 13] that the external priors learned from natural clean images are effective and efficient for image denoising problem, but they are not adaptive to the given noisy image so that some fine-scale image structures may not be well recovered. By contrast, the internal priors are adaptive to content of the given image, but the learning processing are usually slow. In addition, most of the internal prior learning methods [1, 6, 23, 22] assume AWGN noise, making the learned priors less robust for real noisy images. In this paper, we use external priors to guide the internal prior learning. Our method is not only much faster than the traditional internal learning methods, but also very effective to denoise real noisy images.

2.2. Real Noisy Image Denoising

In the last decade, there are many methods [16, 17, 19, 20, 18, 14] for blind image denoising problem. These methods can be applied to real noisy image denoising directly. Liu *et al.* [16] proposed to use “noise level function” to estimate the noise and then use Gaussian conditional random

field to obtain the latent clean image. Gong et al. [17] models the noise by mixed ℓ_1 and ℓ_2 norms and remove the noise by sparsity prior in the wavelet transform domain. Recently, Zhu et al. proposed a Bayesian model [18] which approximates and removes the noise via low-rank mixture of Gaussians. The method of “Noise Clinic” [19, 20] and the software of Neat Image [21] are developed specifically for real noisy image denoising. “Noise Clinic” [19, 20] generalizes the NL-Bayes model [24] to deal with blind noise and achieves state-of-the-art performance. However, these methods largely depends on the modeling of noise in real noisy images which is hard to be modeled by explicit distributions. Besides, the parametric estimation of the Gaussian or MoG distribution is often time consuming.

3. External Prior Guided Internal Prior Learning

In this section, we first describe the learning of external prior, and then describe in detail the guided internal prior learning. Finally, the denoising algorithm with the learned priors is presented.

3.1. Learn External Patch Group Priors

The nonlocal self-similarity based patch group (PG) [7] has proved to be a very effective unit for image prior learning. In this work, we also extract PGs from natural clean images to learn priors. A PG is a group of similar patches to a local patch.

In our method, each local patch is extracted from a RGB image with patch size $p \times p \times 3$. We search the M most similar patches to this local patch (including the local patch itself) in a $W \times W$ local region around it. Each patch is stretched to a patch vector $\mathbf{x}_m \in \mathbb{R}^{3p^2 \times 1}$ to form the PG $\{\mathbf{x}_m\}_{m=1}^M$. The mean vector of this PG is $\boldsymbol{\mu} = \frac{1}{M} \sum_{m=1}^M \mathbf{x}_m$, and the group mean subtracted PG is defined as $\bar{\mathbf{X}} \triangleq \{\bar{\mathbf{x}}_m = \mathbf{x}_m - \boldsymbol{\mu}\}$.

Assume we extract a number of N PGs from a set of external natural images, and the n -th PG is $\bar{\mathbf{Y}}_n \triangleq \{\bar{\mathbf{x}}_{n,m}\}_{m=1}^M, n = 1, \dots, N$. A Gaussian Mixture Model (GMM) is learned to model the PG prior. The overall log-likelihood function is

$$\ln \mathcal{L} = \sum_{n=1}^N \ln \left(\sum_{k=1}^K \pi_k \prod_{m=1}^M \mathcal{N}(\bar{\mathbf{x}}_{n,m} | \boldsymbol{\mu}_k, \Sigma_k) \right). \quad (1)$$

The learning process is similar to the GMM learning in [7, 13]. Finally, a GMM model with K Gaussian components is learned, and the learned parameters include mixture weights $\{\pi_k\}_{k=1}^K$, mean vectors $\{\boldsymbol{\mu}_k\}_{k=1}^K$, and covariance matrices $\{\Sigma_k\}_{k=1}^K$. Note that the mean vector of each cluster is naturally zero, i.e., $\boldsymbol{\mu}_k = \mathbf{0}$.

To better describe the subspace of each Gaussian component, we perform singular value decomposition (SVD) on the covariance matrix:

$$\Sigma_k = \mathbf{U}_k \mathbf{S}_k \mathbf{U}_k^\top. \quad (2)$$

The eigenvector matrices $\{\mathbf{U}_k\}_{k=1}^K$ will be employed as the external orthogonal dictionary to guide the internal dictionary learning in next sub-section. In Fig. 4 (a) and (b), we illustrate an external clean image and one orthogonal dictionary learned via GMM on PGs of the external clean image. The singular values in \mathbf{S}_k reflect the significance of the singular vectors in \mathbf{U}_k . They will also be utilized as prior weights for weighted sparse coding in our denoising algorithm.

3.2. Guided Internal Prior Learning

After the external PG prior is learned, we employ it to guide the internal PG prior learning for a given real noisy image. The guidance lies in two aspects. One is that the external prior can guide the subspace assignment of internal noisy PGs, while the other is that the external prior could guide the orthogonal dictionary learning of internal noisy PGs.

3.2.1 Internal Subspace Assignment

Given a real noisy image, we extract N (overlapped) local patches from it. Similar to the external prior learning stage, for the n -th local patch we search its M most similar patches around it to form a noisy PG, denoted by $\mathbf{Y}_n = \{\mathbf{y}_{n,1}, \dots, \mathbf{y}_{n,M}\}$. Then the group mean of \mathbf{Y}_n , denoted by $\boldsymbol{\mu}_n$, is subtracted from each patch by $\bar{\mathbf{y}}_{n,m} = \mathbf{y}_{n,m} - \boldsymbol{\mu}_n$, leading to the mean subtracted noisy PG $\bar{\mathbf{Y}}_n \triangleq \{\bar{\mathbf{y}}_{n,m}\}_{m=1}^M$.

The external GMM prior models $\{\Sigma_k\}_{k=1}^K$ basically characterize the subspaces of natural high quality PGs. Therefore, we project the noisy PG $\bar{\mathbf{Y}}_n$ into the subspaces of $\{\Sigma_k\}_{k=1}^K$ and assign it to the most suitable subspace based on the posterior probability:

$$P(k|\bar{\mathbf{Y}}_n) = \frac{\prod_{m=1}^M \mathcal{N}(\bar{\mathbf{y}}_{n,m} | \mathbf{0}, \Sigma_k)}{\sum_{l=1}^K \prod_{m=1}^M \mathcal{N}(\bar{\mathbf{y}}_{n,m} | \mathbf{0}, \Sigma_l)} \quad (3)$$

for $k = 1, \dots, K$. Then $\bar{\mathbf{Y}}_n$ is assigned to the component with the maximum A-posteriori (MAP) probability $\max_k P(k|\bar{\mathbf{Y}}_n)$.

3.2.2 Guided Orthogonal Dictionary Learning

Assume we have assigned all internal noisy PGs $\{\bar{\mathbf{Y}}_n\}_{n=1}^N$ to their corresponding most suitable Gaussians or subspaces in $\{\mathcal{N}(\mathbf{0}, \Sigma_k)\}_{k=1}^K$. For the k -th subspace, assume the noisy PGs assigned to it are $\{\bar{\mathbf{Y}}_{k,n}\}_{n=1}^{N_k}$ such that $\bar{\mathbf{Y}}_{k,n} = [\bar{\mathbf{y}}_{k,n,1}, \dots, \bar{\mathbf{y}}_{k,n,M}]$ and $\sum_{n=1}^{N_k} N_k = N$. We utilize the external orthogonal dictionary \mathbf{U}_k (Eqn. (2)) to guide the learning of an orthogonal dictionary for adaptively characterizing the internal PGs in the k -th subspace. The reasons we aim to learn orthogonal dictionaries are two-fold: firstly, given an orthonormal dictionary \mathbf{D} , its quality measure *mutual incoherence* $\mu(\mathbf{D}) = \max_{i=j} \frac{|\mathbf{d}_i^\top \mathbf{d}_j|}{\|\mathbf{d}_i\|_2 \|\mathbf{d}_j\|_2}$ is naturally 0

324 and therefore better than other redundant dictionaries; sec-
 325 ondly, the orthogonality of dictioanry can guarantee the dictio-
 326 nary learning stage has closed-form solutions (please refer to Eqn. (9)) and the closed-form solutions will make our
 327 proposed method efficient, which will be discussed in ex-
 328 perimental section.
 329

330 The learned dictionary $\mathbf{D}_k \triangleq [\mathbf{D}_{k,e} \ \mathbf{D}_{k,i}] \in \mathbb{R}^{3p^2 \times 3p^2}$
 331 has two parts: the external part $\mathbf{D}_{k,e} = \mathbf{U}_k(:, 1 : 3p^2 - r) \in \mathbb{R}^{3p^2 \times (3p^2 - r)}$ is directly obtained from the external dictio-
 332 nary \mathbf{U}_k , and the internal part $\mathbf{D}_{k,i}$ is consisted of dictio-
 333 nary atoms adaptively learned from the internal noisy PGs
 334 $\{\bar{\mathbf{Y}}_{k,n}\}_{n=1}^{N_k}$. For notation simplicity, we ignore the subspace
 335 index k and denote the noisy PGs assigned to each subspace
 336 as $\mathbf{Y} \triangleq \{\bar{\mathbf{Y}}_n\}_{n=1}^N = [\bar{\mathbf{y}}_{1,1}, \dots, \bar{\mathbf{y}}_{1,M}, \dots, \bar{\mathbf{y}}_{N,1}, \dots, \bar{\mathbf{y}}_{N,M}]$. The learning is performed under the weighted sparse cod-
 337 ing framework proposed as follows:
 338

$$\begin{aligned} & \min_{\mathbf{D}_i, \{\alpha_{n,m}\}} \sum_{n=1}^N \sum_{m=1}^M (\|\bar{\mathbf{y}}_{n,m} - \mathbf{D}\alpha_{n,m}\|_2^2 + \sum_{j=1}^{3p^2} \lambda_j |\alpha_{n,m,j}|) \\ & \text{s.t. } \mathbf{D} = [\mathbf{D}_e \ \mathbf{D}_i], \mathbf{D}_i^\top \mathbf{D}_i = \mathbf{I}_r, \mathbf{D}_e^\top \mathbf{D}_i = \mathbf{0}, \end{aligned} \quad (4)$$

339 where $\alpha_{n,m}$ is the sparse coefficient vector of the m -th
 340 patch $\bar{\mathbf{y}}_{n,m}$ in the n -th PG $\bar{\mathbf{Y}}_n$ and $\alpha_{n,m,j}$ is the j -th element of $\alpha_{n,m}$. λ_j is the j -th regularization parameter de-
 341 fined as
 342

$$\lambda_j = \lambda / (\sqrt{\mathbf{S}_j} + \varepsilon). \quad (5)$$

343 We employ square roots of the singular values in \mathbf{S} (please
 344 refer to Eqn. (2)) as external prior weights and add a small
 345 positive number ε to avoid zero denominator. Noted that
 346 $\mathbf{D}_e = \emptyset$ if $r = 3p^2$ and $\mathbf{D}_e = \mathbf{U}_k$ if $r = 0$. The dictionary
 347 $\mathbf{D} = [\mathbf{D}_e \ \mathbf{D}_i]$ is orthogonal by checking that:
 348

$$\mathbf{D}^\top \mathbf{D} = \begin{bmatrix} \mathbf{D}_e^\top \\ \mathbf{D}_i^\top \end{bmatrix} [\mathbf{D}_e \ \mathbf{D}_i] = \begin{bmatrix} \mathbf{D}_e^\top \mathbf{D}_e & \mathbf{D}_e^\top \mathbf{D}_i \\ \mathbf{D}_i^\top \mathbf{D}_e & \mathbf{D}_i^\top \mathbf{D}_i \end{bmatrix} = \mathbf{I} \quad (6)$$

349 Similar to K-SVD [1], we employ an alternating iterative
 350 framework to solve the optimization problem (5). Specifically,
 351 we initialize the orthogonal dictionary as $\mathbf{D}_{(0)} = \mathbf{U}_k$
 352 and for $t = 0, 1, \dots, T - 1$, alternatively do:
 353

354 **Updating Sparse Coefficient:** given the orthogonal dictio-
 355 nary $\mathbf{D}_{(t)}$, we update the sparse coefficient vector of the m -
 356 th patch $\bar{\mathbf{y}}_{n,m}$ in the n -th PG $\bar{\mathbf{Y}}_n$ via solving
 357

$$\begin{aligned} & \alpha_{n,m}^{(t)} := \arg \min_{\alpha_{n,m}} \|\bar{\mathbf{y}}_{n,m} - \mathbf{D}_{(t)} \alpha_{n,m}\|_2^2 + \sum_{j=1}^{3p^2} \lambda_j |\alpha_{n,m,j}| \\ & \text{s.t. } \mathbf{D}_{(t)} = [\mathbf{D}_e \ \mathbf{D}_i], \mathbf{D}_i^\top \mathbf{D}_i = \mathbf{I}_r, \mathbf{D}_e^\top \mathbf{D}_i = \mathbf{0}, \end{aligned} \quad (7)$$

358 Since dictionary $\mathbf{D}_{(t)} = [\mathbf{D}_e \ \mathbf{D}_i^{(t)}]$ is orthogonal, the prob-
 359 lems (7) has a closed-form solution [7]
 360

$$\alpha_{n,m}^{(t)} = \text{sgn}(\mathbf{D}_{(t)}^\top \bar{\mathbf{y}}_{n,m}) \odot \max(|\mathbf{D}_{(t)}^\top \bar{\mathbf{y}}_{n,m}| - \Lambda, 0), \quad (8)$$

361 where $\Lambda = [\lambda_1, \lambda_2, \dots, \lambda_{3p^2}]$ is the vector of regulariza-
 362 tion parameter and $\text{sgn}(\bullet)$ is the sign function, \odot means
 363

364 element-wise multiplication.
 365

366 **Updating Internal Dictionary:** given the sparse coeffi-
 367 cient vectors $\mathbf{A}^{(t)} = [\alpha_{1,1}^{(t)}, \dots, \alpha_{1,M}^{(t)}, \dots, \alpha_{N,1}^{(t)}, \dots, \alpha_{N,M}^{(t)}]$,
 368 we update the internal orthogonal dictionary via solving
 369

$$\begin{aligned} \mathbf{D}_i^{(t+1)} &:= \arg \min_{\mathbf{D}_i} \sum_{n=1}^N \sum_{m=1}^M (\|\bar{\mathbf{y}}_{n,m} - \mathbf{D}\alpha_{n,m}\|_2^2) \\ &= \arg \min_{\mathbf{D}_i} \|\mathbf{Y} - \mathbf{D}\mathbf{A}^{(t)}\|_F^2 \end{aligned} \quad (9)$$

$$\text{s.t. } \mathbf{D} = [\mathbf{D}_e \ \mathbf{D}_i], \mathbf{D}_i^\top \mathbf{D}_i = \mathbf{I}_r, \mathbf{D}_e^\top \mathbf{D}_i = \mathbf{0},$$

370 The sparse coefficient matrix $\mathbf{A}^{(t)} = [(\mathbf{A}_e^{(t)})^\top \ (\mathbf{A}_i^{(t)})^\top]^\top$
 371 also has two parts: the external part $\mathbf{A}_e^{(t)} \in \mathbb{R}^{(3p^2 - r) \times NM}$
 372 and the internal part $\mathbf{A}_i^{(t)} \in \mathbb{R}^{r \times NM}$ denote the coefficients
 373 over external dictionary \mathbf{D}_e and internal dictionary $\mathbf{D}_i^{(t)}$,
 374 respectively. According to the Theorem 4 in [25], the prob-
 375 lem (9) has a closed-form solution $\mathbf{D}_i^{(t+1)} = \mathbf{U}_i \mathbf{V}_i^\top$, where
 376 $\mathbf{U}_i \in \mathbb{R}^{3p^2 \times r}$ and $\mathbf{V}_i \in \mathbb{R}^{r \times r}$ are the orthogonal matrices
 377 obtained by the following SVD

$$(\mathbf{I} - \mathbf{D}_e \mathbf{D}_e^\top) \mathbf{Y} (\mathbf{A}_i^{(t)})^\top = \mathbf{U}_i \mathbf{S}_i \mathbf{V}_i^\top. \quad (10)$$

378 The orthogonality of internal dictionary $\mathbf{D}_i^{(t+1)}$ can be
 379 checked by $(\mathbf{D}_i^{(t+1)})^\top (\mathbf{D}_i^{(t+1)}) = \mathbf{V}_i \mathbf{U}_i^\top \mathbf{U}_i \mathbf{V}_i^\top = \mathbf{I}_r$.
 380 In Figure 4 (c) and (d), we illustrate a denoised image by
 381 our proposed method and one internal orthogonal dictionary
 382 learned from PGs of the given noisy image.
 383

3.3. The Denoising Algorithm

384 We evaluate the performance of the proposed framework
 385 on denoising real noisy images. The denoising is simultane-
 386 ously done with the guided internal dictionary learning
 387 process. We ignore the index $k \in \{1, \dots, K\}$ of subspace
 388 for notation simplicity. In the denoising stage, for each sub-
 389 space, the group mean vectors $\{\mu_n\}_{n=1}^N$ of corresponding
 390 mean subtracted noisy PGs $\{\bar{\mathbf{Y}}_n\}_{n=1}^N$ are saved for recon-
 391 struction. Until now, we obtain the solutions of sparse coef-
 392 ficient vectors $\{\hat{\alpha}_{n,m}^{(T-1)}\}$ in Eqn. (8) for $n = 1, \dots, N; m =$
 393 $1, \dots, M$ and the orthogonal dictionary $\mathbf{D}_{(T)} = [\mathbf{D}_e \ \mathbf{D}_i^{(T)}]$
 394 in Eqn. (9). Then the m -th latent clean patch $\hat{\mathbf{y}}_{n,m}$ in the
 395 n -th PG $\bar{\mathbf{Y}}_n$ is recovered by
 396

$$\hat{\mathbf{y}}_{n,m} = \mathbf{D}_{(T)} \hat{\alpha}_{n,m} + \mu_n, \quad (11)$$

397 where $n = 1, \dots, N; m = 1, \dots, M$. The latent clean im-
 398 age $\hat{\mathbf{x}}$ is reconstructed by aggregating all the estimated PGs.
 399 Similar to [7], we perform the above denoising procedures
 400 for several iterations for better denoising outputs. The pro-
 401 posed denoising algorithm is summarized in Alg. 1.
 402

4. Experiments

403 In this section, we evaluate the performance of the pro-
 404 posed algorithm on real image denoising. To evaluation the
 405 effectiveness of the proposed framework of external prior
 406

432 **Alg. 1:** External Prior Guided Internal Prior Learning
 433 for Real Noisy Image Denoising
 434
 435 **Input:** Noisy image y , external PG prior GMM model
 436 **Output:** The denoised image \hat{x} .
 437 **Initialization:** $\hat{x}^{(0)} = y$;
 438 **for** $Ite = 1 : IteNum$ **do**
 439 1. Extracting internal PGs from $\hat{x}^{(Ite-1)}$;
 440 **for** each PG Y_n **do**
 441 2. Calculate group mean vector μ_n and form
 442 mean subtracted PG \bar{Y}_n ;
 443 3. Subspace selection via Eqn. (3);
 444 **end for**
 445 **for** the PGs in each Subspace **do**
 446 4. External PG prior Guided Internal Orthogonal
 447 Dictionary Learning by solving (4);
 448 5. Recover each patch in all PGs via Eqn. (11);
 449 **end for**
 450 6. Aggregate the recovered PGs of all subspaces to form
 451 the recovered image $\hat{x}^{(Ite)}$;
 452 **end for**

453
 454 guided internal prior learning, we compare it with the methods
 455 with only external prior or only internal prior (Section
 456 4.3). We also compare the proposed algorithm with other
 457 state-of-the-art denoising methods [4, 5, 9, 8, 10, 11, 14,
 458 19, 20, 21] (Section 4.4).

4.1. The Testing Datasets

460 The comparisons are performed on two standard datasets
 461 in which the images were captured under indoor or outdoor
 462 lighting conditions by different types of cameras and
 463 camera settings. The first dataset provided in [20] includes
 464 20 real noisy images collected under uncontrolled outdoor
 465 environment. This dataset does not have “ground truth”
 466 images and hence the objective measurements can not be
 467 performed. In order to evaluate the compared methods on
 468 quantitative measures, we perform experiments on the sec-
 469 ond dataset provided in [14]. It includes 17 real noisy im-
 470 ages and corresponding mean images. The noisy images
 471 were collected under controlled indoor environment. Some
 472 samples can be found in [14]. For each image, the same
 473 scene was shot 500 times under the same camera and cam-
 474 era setting. The mean image of the 500 shots is roughly
 475 taken as the “ground truth”, with which the PSNR can be
 476 computed. Since the 17 images are too large (of size about
 477 $7000 \times 5000 \times 3$) and share repetitive contents, the authors in
 478 [14] performed comparison on 15 cropped images (of size
 479 $512 \times 512 \times 3$). To evaluate the compared methods on more
 480 samples, we cropped the 17 large images from [14] into 60
 481 smaller images (of size $500 \times 500 \times 3$) including different
 482 contents. Some samples are shown in Figure 5. Note that
 483 the noise in our cropped 60 images used in [14] are different
 484
 485

486 from the noise in the 15 images cropped by the authors of
 487 [14] since they are taken in different shots.
 488

4.2. Implementation Details

489 Our proposed method contains two stages, the external
 490 prior learning stage and the external prior guided internal
 491 learning stage. In the first stage, we set $p = 6$ (so the
 492 patch size is $6 \times 6 \times 3$), $M = 10$ (the number of patches
 493 in a patch group (PG)), $W = 31$ (so the window size for
 494 PG searching is 31×31 , and $K = 32$ (the number of
 495 Gaussians in Gaussian Mixture Model (GMM)). We learn
 496 the external prior via GMM on about 3.6 million PGs ex-
 497 tracted from the Kodak PhotoCD Dataset (<http://r0k.us/graphics/kodak/>), which includes 24 high quality
 498 color images. In the second stage, we set $r = 54$ (the num-
 499 ber of internal atoms in the learned dictionaries), $\lambda = 0.001$
 500 (the sparse regularization parameter), $T = 2$ (the num-
 501 ber of iterations for solving problem (4)), and $IteNum = 4$
 502 (the number of iterations for Alg. 1). All experiments are
 503 performed under the Matlab2014b environment on a ma-
 504 chine with Intel(R) Core(TM) i7-5930K CPU of 3.5GHz
 505 and 32GB RAM.
 506
 507

4.3. Comparison among external, internal and external guided internal priors

508 In this section, we compare our proposed method on real
 509 image denoising with external prior based method (denoted
 510 as “External”) and internal prior based method (denoted as
 511 “Internal”). For the “External” method, we utilize the ex-
 512 ternal dictionaries (i.e., $r = 0$ in Eqn. (5)) for denoising.
 513 For the given noisy image, we extract the PGs and then do
 514 internal subspace selection via Eqn. 3. The denoising is per-
 515 formed via the weighted sparse coding framework proposed
 516 in [7]. For the “Internal” method, the overall framework is
 517 similar to the method of [6]. We employ the GMM model
 518 (also with $K = 32$ Gaussians) to cluster the noisy PGs
 519 extracted from given noisy image into multiple subspaces,
 520 and for each subspace, we utilize the internal orthogonal
 521 dictionary obtained via Eqn. (2) by weighted sparse coding
 522 framework in [7]. All parameters of the three methods are
 523 tuned to achieve best performance.
 524
 525

526 We compare the above mentioned methods on the 60
 527 cropped images (of size $500 \times 500 \times 3$) from [14]. The
 528 average PSNR and speed of these methods are listed in Ta-
 529 ble 1. It can be seen that our proposed method achieves
 530 better PSNR results than the methods of “External” and “In-
 531 ternal”. The speed of our proposed method is much faster
 532 than the “Internal” method while only a little slower than
 533 the “External” method. We also compare the visual quality
 534 of the denoised images by these methods. From the results
 535 listed in Figure 3 and Figure 4, we can see that the “Ex-
 536 ternal” method is good at recovering structures (Figure 3)
 537 while the “Internal” method is good at recovering internal
 538
 539

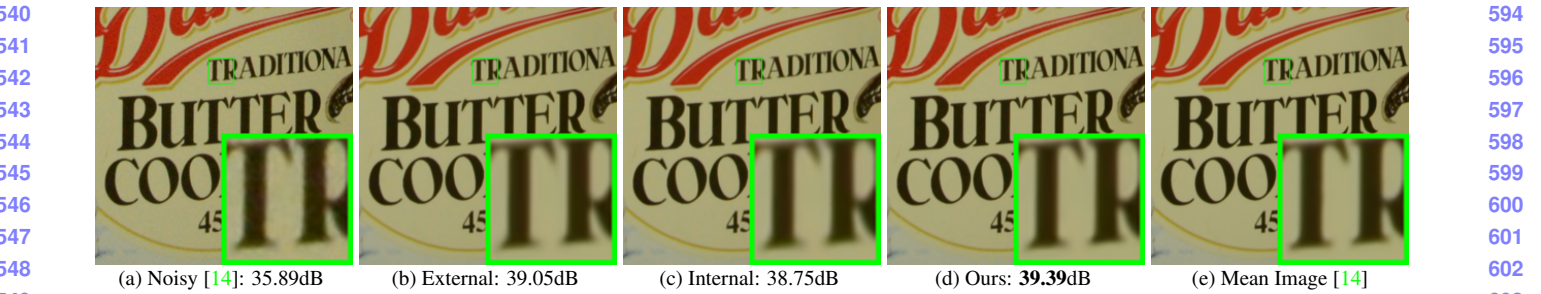


Figure 3. Denoised images of the 96-th cropped image from “Nikon D600 ISO 3200 C1” [14] by different methods. The images are better to be zoomed in on screen.

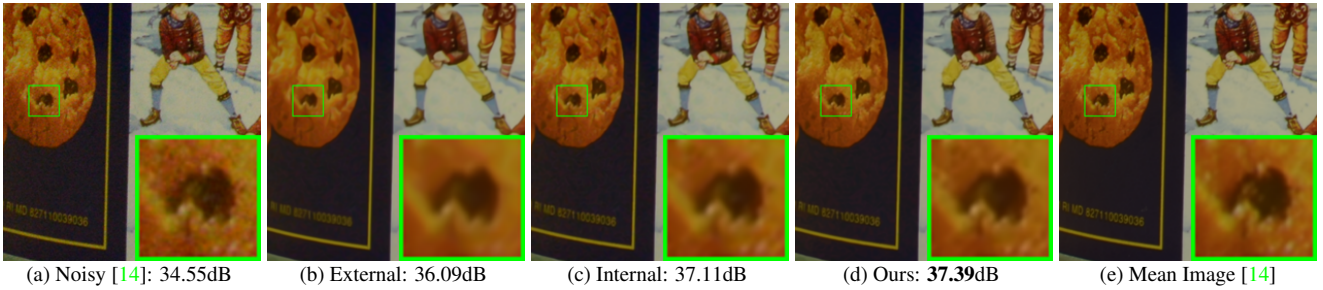


Figure 4. Denoised images of the 94-th cropped image from “Nikon D600 ISO 3200 C1” [14] by different methods. The images are better to be zoomed in on screen.



Figure 5. Some samples cropped from real noisy images of [14].

Table 1. Average PSNR (dB) results and Run Time (seconds) of the External, the Internal, and our proposed methods on 60 real noisy images (of size $500 \times 500 \times 3$) cropped from [14].

	Noisy	External	Internal	Ours
PSNR	34.51	38.21	38.07	38.75
Time	—	39.57	667.36	41.89

complex textures (Figure 4). And by utilizing both the external and internal priors, our proposed method can recover well both the structures and textures. Noted that the noisy images in Figures 3 and 4 are cropped from the same image captured by Nikon D600 at ISO = 3200 in [14]. Hence, the differences on PSNR and visual quality among these methods only depends on the contents of the cropped images.

4.4. Comparison with Other Denoising Methods

In this section, we compare the proposed method with other state-of-the-art image denoising methods such as BM3D [4], WNNM [8], MLP [9], CSF [10], TRD [11], Noise Clinic (NC) [19], Cross-Channel (CC) [14], and Neat Image (NI) [21]. The methods of BM3D [4], WNNM [8], MLP [9], CSF [10], and TRD [11] are designed for removing Gaussian noise. For BM3D and WNNM, the level σ of Gaussian noise is very important and is estimated by

the method [26]. The other parameters are set as default. For the methods of MLP, CSF, and TRD, we employ their default parameters settings. Since these methods are designed for grayscale images, we utilize them to denoise the R, G, B channels separately for color noisy images. The Noise Clinic (NC) [19] is a blind image denoising method which does not need any noise prior. We also compare with Neat Image (NI), a commercial software for image denoising. Due to its excellent performance, Neat Image (NI) is embedded into Photoshop and Corel PaintShop [21]. The comparisons are performed on the real noisy images from [20] and [14].

4.4.1 Comparison on the First Dataset [20]

The real noisy images in the dataset [20] do not have “ground truth” images. On this dataset, we compare the proposed method with the methods of BM3D [4], WNNM [8], MLP [9], TRD [11], Noise Clinic (NC) [19], and Neat Image (NI) [21]. We only compare the visual quality of the denoised images. Figure 6 shows the denoised images of “Dog” by the competing methods. More visual comparisons can be found in the supplementary file. It can be seen that the methods of BM3D, WNNM tend to globally oversmooth the image while locally remain some noise, while the methods of MLP, TRD are likely to remain noise in the whole image. This demonstrates that the methods designed for Gaussian noise are not effective for removing the complex noise in real noisy images. Though Noise Clinic and Neat Image are specifically developed for removing complex noise, they would sometimes fail to recover real noisy

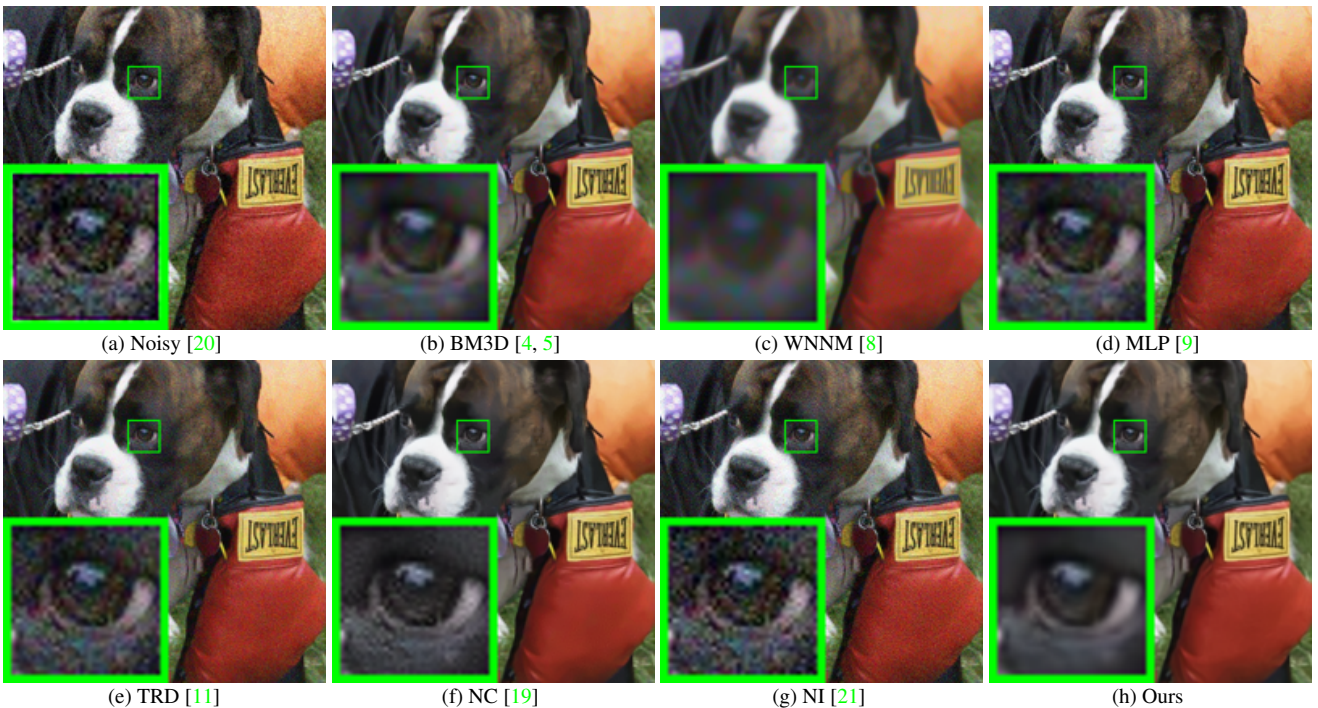


Figure 6. Denoised images of the image “Dog” by different methods. The images are better to be zoomed in on screen.

images. However, our proposed method recoveries more faithfully the structures and textures (such as the eye area) than the other competing methods.

4.4.2 Comparison on the Second Dataset [14]

The real noisy images in the second dataset [14] have corresponding “ground truth” images. On this dataset, we firstly perform comparison on the 15 cropped images used in [14]. The compared method are BM3D [4], WNNM [8], MLP [9], CSF [10], TRD [11], Noise Clinic (NC) [19], and Cross-Channel (CC) [14]. The PSNR values are listed in Table 2. As we can see, on most (9 out of the 15) images captured by different cameras and camera settings, our proposed method obtains better PSNR values than the other methods. Noted that, though in [14] a specific model is trained for each camera and camera setting, our proposed general method still gains 0.28dB improvements on PNSR over [14]. We also compare the visual quality of the denoised images by the competing methods. Figure 7 shows the denoised images of a scene captured by Canon 5D Mark 3 at ISO = 3200 by the competing methods. More visual comparisons can be found in the supplementary file. We can see that BM3D, WNNM, NC, NI, and CC would either remain noise or generate artifacts, while MLP, TRD are likely to over-smooth the image. By combining the external and internal priors, our proposed method preserves edges and textures better than other methods.

To evaluate the compared methods on more samples, we

then perform denoising experiments on the 60 smaller images cropped from the 17 images provided in [14]. The average PSNR results are listed in Table 3 (the code of [14] is not available so that it is not compared). The numbers in red color and blue color are the best and second best results, respectively. It can be seen that our proposed method achieves much better PSNR results than the other methods. The improvement of our method over the second best method (TRD) is 1dB. Due to the spacial limitations, the visual comparisions are provided in the supplementary file.

5. Conclusion and Future Work

Image priors are important for solving image denoising problems. The external priors learned from external clean images are generally effective to most images, while the internal priors learned directly from the noisy image are adaptive to the given image but would be biased by the complex noise in real noisy images. In this paper, we demonstrates that, once unifying both the priors in external clean images and internal noisy images, we can achieve much better while still efficient performance on real image denoising problem. Specifically, the external patch group (PG) priors learned on natural clean images can be used to guide the subspace selection and orthogonal dictionary learning of internal noisy PGs from given noisy images. The experiments on real image denoising problem have demonstrated the powerful ability of the proposed method. In the future, we will speed up the proposed algorithm and evaluate the

Table 2. Average PSNR(dB) results of different methods on 15 cropped real noisy images used in [14].

Camera Settings	Noisy	BM3D	WNNM	MLP	CSF	TRD	NI	NC	CC	Ours
Canon 5D Mark III ISO = 3200	37.00	37.08	37.09	33.92	35.68	36.20	37.68	38.76	38.37	40.50
	33.88	33.94	33.93	33.24	34.03	34.35	34.87	35.69	35.37	37.05
	33.83	33.88	33.90	32.37	32.63	33.10	34.77	35.54	34.91	36.11
Nikon D600 ISO = 3200	33.28	33.33	33.34	31.93	31.78	32.28	34.12	35.57	34.98	34.88
	33.77	33.85	33.79	34.15	35.16	35.34	35.36	36.70	35.95	36.31
	34.93	35.02	34.95	37.89	39.98	40.51	38.68	39.28	41.15	39.23
Nikon D800 ISO = 1600	35.47	35.54	35.57	33.77	34.84	35.09	37.34	38.01	37.99	38.40
	35.71	35.79	35.77	35.89	38.42	38.65	38.57	39.05	40.36	40.92
	34.81	34.92	34.95	34.25	35.79	35.85	37.87	38.20	38.30	38.97
Nikon D800 ISO = 3200	33.26	33.34	33.31	37.42	38.36	38.56	36.95	38.07	39.01	38.66
	32.89	32.95	32.96	34.88	35.53	35.76	35.09	35.72	36.75	37.07
	32.91	32.98	32.96	38.54	40.05	40.59	36.91	36.76	39.06	38.52
Nikon D800 ISO = 6400	29.63	29.66	29.71	33.59	34.08	34.25	31.28	33.49	34.61	33.76
	29.97	30.01	29.98	31.55	32.13	32.38	31.38	32.79	33.21	33.43
	29.87	29.90	29.95	31.42	31.52	31.76	31.40	32.86	33.22	33.58
Average	33.41	33.48	33.48	34.32	35.33	35.65	35.49	36.43	36.88	37.16

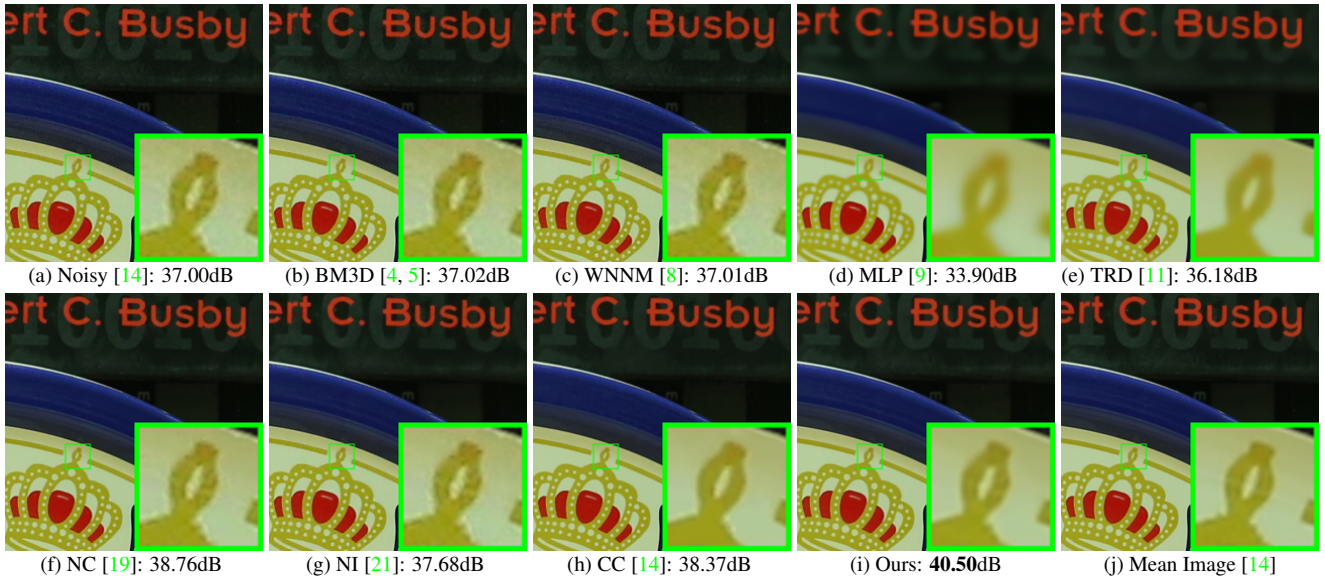


Figure 7. Denoised images of the image “Canon 5D Mark 3 ISO 3200 1” by different methods. The images are better to be zoomed in on screen.

Table 3. Average PSNR(dB) results of different methods on 60 real noisy images cropped from [14].

Methods	BM3D	WNNM	MLP	CSF
PSNR	34.58	34.52	36.19	37.40
Methods	TRD	NI	NC	Ours
PSNR	37.75	36.53	37.57	38.75

proposed method on other computer vision tasks such as image super-resolution.

864
865
866
867
868
869

References

- [1] M. Elad and M. Aharon. Image denoising via sparse and redundant representations over learned dictionaries. *IEEE Transactions on Image Processing*, 15(12):3736–3745, 2006. 1, 2, 4
- [2] J. Mairal, F. Bach, J. Ponce, G. Sapiro, and A. Zisserman. Non-local sparse models for image restoration. *IEEE International Conference on Computer Vision (ICCV)*, pages 2272–2279, 2009. 1
- [3] A. Buades, B. Coll, and J. M. Morel. A non-local algorithm for image denoising. *IEEE Conference on Computer Vision and Pattern Recognition (CVPR)*, pages 60–65, 2005. 1
- [4] K. Dabov, A. Foi, V. Katkovnik, and K. Egiazarian. Image denoising by sparse 3-D transform-domain collaborative filtering. *IEEE Transactions on Image Processing*, 16(8):2080–2095, 2007. 1, 2, 5, 6, 7, 8
- [5] K. Dabov, A. Foi, V. Katkovnik, and K. Egiazarian. Color image denoising via sparse 3D collaborative filtering with grouping constraint in luminance-chrominance space. *IEEE International Conference on Image Processing (ICIP)*, pages 313–316, 2007. 1, 2, 5, 7, 8
- [6] W. Dong, L. Zhang, G. Shi, and X. Li. Nonlocally centralized sparse representation for image restoration. *IEEE Transactions on Image Processing*, 22(4):1620–1630, 2013. 1, 2, 5
- [7] J. Xu, L. Zhang, W. Zuo, D. Zhang, and X. Feng. Patch group based nonlocal self-similarity prior learning for image denoising. *IEEE International Conference on Computer Vision (ICCV)*, pages 244–252, 2015. 1, 2, 3, 4, 5
- [8] S. Gu, L. Zhang, W. Zuo, and X. Feng. Weighted nuclear norm minimization with application to image denoising. *IEEE Conference on Computer Vision and Pattern Recognition (CVPR)*, pages 2862–2869, 2014. 1, 2, 5, 6, 7, 8
- [9] H. C. Burger, C. J. Schuler, and S. Harmeling. Image denoising: Can plain neural networks compete with BM3D? *IEEE Conference on Computer Vision and Pattern Recognition (CVPR)*, pages 2392–2399, 2012. 1, 2, 5, 6, 7, 8
- [10] U. Schmidt and S. Roth. Shrinkage fields for effective image restoration. *IEEE Conference on Computer Vision and Pattern Recognition (CVPR)*, pages 2774–2781, June 2014. 1, 2, 5, 6, 7
- [11] Y. Chen, W. Yu, and T. Pock. On learning optimized reaction diffusion processes for effective image restoration. *IEEE Conference on Computer Vision and Pattern Recognition (CVPR)*, pages 5261–5269, 2015. 1, 2, 5, 6, 7, 8
- [12] S. Roth and M. J. Black. Fields of experts. *International Journal of Computer Vision*, 82(2):205–229, 2009. 1, 2
- [13] D. Zoran and Y. Weiss. From learning models of natural image patches to whole image restoration. *IEEE International Conference on Computer Vision (ICCV)*, pages 479–486, 2011. 1, 2, 3
- [14] S. Nam, Y. Hwang, Y. Matsushita, and S. J. Kim. A holistic approach to cross-channel image noise modeling and its application to image denoising. *IEEE Conference on Computer Vision and Pattern Recognition (CVPR)*, pages 1683–1691, 2016. 1, 2, 5, 6, 7, 8
- [15] G. E Healey and R. Kondepudy. Radiometric CCD camera calibration and noise estimation. *IEEE Transactions on Pattern Analysis and Machine Intelligence*, 16(3):267–276, 1994. 1
- [16] C. Liu, R. Szeliski, S. Bing Kang, C. L. Zitnick, and W. T. Freeman. Automatic estimation and removal of noise from a single image. *IEEE Transactions on Pattern Analysis and Machine Intelligence*, 30(2):299–314, 2008. 1, 2
- [17] Z. Gong, Z. Shen, and K.-C. Toh. Image restoration with mixed or unknown noises. *Multiscale Modeling & Simulation*, 12(2):458–487, 2014. 1, 2, 3
- [18] F. Zhu, G. Chen, and P.-A. Heng. From noise modeling to blind image denoising. *IEEE Conference on Computer Vision and Pattern Recognition (CVPR)*, June 2016. 1, 2, 3
- [19] M. Lebrun, M. Colom, and J.-M. Morel. Multiscale image blind denoising. *IEEE Transactions on Image Processing*, 24(10):3149–3161, 2015. 1, 2, 3, 5, 6, 7, 8
- [20] M. Lebrun, M. Colom, and J. M. Morel. The noise clinic: a blind image denoising algorithm. <http://www.ipol.im/pub/art/2015/125/>. Accessed 01 28, 2015. 1, 2, 3, 5, 6, 7
- [21] Neatlab ABSoft. Neat Image. <https://ni.neatvideo.com/home>. 1, 2, 3, 5, 6, 7, 8
- [22] M. Zontak and M. Irani. Internal statistics of a single natural image. *IEEE Conference on Computer Vision and Pattern Recognition (CVPR)*, pages 977–984, 2011. 2
- [23] G. Yu, G. Sapiro, and S. Mallat. Solving inverse problems with piecewise linear estimators: From Gaussian mixture models to structured sparsity. *IEEE Transactions on Image Processing*, 21(5):2481–2499, 2012. 2
- [24] M. Lebrun, A. Buades, and J. M. Morel. A nonlocal Bayesian image denoising algorithm. *SIAM Journal on Imaging Sciences*, 6(3):1665–1688, 2013. 3
- [25] H. Zou, T. Hastie, and R. Tibshirani. Sparse principal component analysis. *Journal of Computational and Graphical Statistics*, 15(2):265–286, 2006. 4
- [26] X. Liu, M. Tanaka, and M. Okutomi. Single-image noise level estimation for blind denoising. *IEEE transactions on Image Processing*, 22(12):5226–5237, 2013. 6

918
919
920
921
922
923
924
925
926
927
928
929
930
931
932
933
934
935
936
937
938
939
940
941
942
943
944
945
946
947
948
949
950
951
952
953
954
955
956
957
958
959
960
961
962
963
964
965
966
967
968
969
970
971